Synaptic Transmission at Visualized Sympathetic Boutons: Stochastic Interaction Between Acetylcholine and Its Receptors

M. R. Bennett,* L. Farnell,# W. G. Gibson,# and N. A. Lavidis*
*Neurobiology Laboratory, Department of Physiology, and Sydney Institute for Biomedical Research; and #School of Mathematics and Statistics, University of Sydney, New South Wales 2006, Australia

ABSTRACT Excitatory postsynaptic currents (EPSCs) were recorded with loose patch electrodes placed over visualized boutons on the surface of rat pelvic ganglion cells. At 34°C the time to peak of the EPSC was about 0.7 ms, and a single exponential described the declining phase with a time constant of about 4.0 ms; these times were not correlated with changes in the amplitude of the EPSC. The amplitude-frequency histogram of the EPSC at individual boutons was well described by a single Gaussian distribution that possessed a variance similar to that of the electrical noise. Nonstationary fluctuation analysis of the EPSCs at a bouton indicated that about 120 ACh receptor channels were available beneath boutons for interaction with a quantum of ACh. The characteristics of these EPSCs were compared with the results of Monte Carlo simulations of the quantal release of 9000 acetylcholine (ACh) molecules onto receptor patches of density 1400 μm^{-2} and 0.41 μm diameter, using a kinetic scheme of interaction between ACh and the receptors similar to that observed at the neuromuscular junction. The simulated EPSC generated in this way had temporal characteristics similar to those of the experimental EPSC when either the diffusion of the ACh is slowed or allowance is made for a finite period of transmitter release from the bouton. The amplitude of the simulated EPSC then exhibited stochastic fluctuations similar to those of the experimental EPSC.

INTRODUCTION

The interaction between acetylcholine (ACh) released from a bouton on an autonomic ganglion cell and its receptors has traditionally been studied by analyzing the time course of the spontaneous excitatory postsynaptic current (SEPSC) under the assumption that this current arises from the secretion of a quantum of transmitter from a single bouton (see, for example, Rang, 1981). Such approaches have given rise to the idea that the 10,000 or so molecules of ACh in a synaptic vesicle (Whittaker, 1990) constitute a quantum that saturates a small number of receptors beneath a bouton (on the order of 100: Rang, 1981; Dryer and Chiappinelli, 1987). However, the amplitude-frequency histogram of SEPSCs is not described by a Gaussian distribution, as are the spontaneous synaptic currents at the motor endplate; a more appropriate distribution is one that is positively skewed, such as a gamma distribution or a Poisson mixture of Gaussians (see, for example, Bornstein, 1978; Martin and Pilar, 1964; Warren et al., 1995a). This raises questions as to whether there is spontaneous quantal release of transmitter (for a review of this problem see Bennett, 1995). In some cases there is evidence of spontaneous multiquantal release, suggesting that there is either synchronous release of quanta from adjacent boutons or multiquantal release from a single bouton (Bennett et al., 1995b).

In the present work we have avoided the complexity introduced by these possibilities by studying transmitter release from single visualized boutons in the rat pelvic ganglion. This preparation consists of monopolar neurons that mostly receive innervation from a single nerve terminal that breaks up into about 20 boutons on the soma of the neurons (Tabatabai et al., 1986; de Groat and Booth, 1993; Yakota and Burnstock, 1983). Individual boutons can easily be identified, for use in recording the electrical signs of transmission with a loose patch electrode, by $DiOC_2(5)$ fluorescent staining of mitochondria in the boutons (as for the varicosities of their sympathetic nerve terminals; Lavidis and Bennett, 1992), by orthograde labeling of the boutons with dextran coupled to rhodamine (Warren et al., 1995b), or by use of the fluorescent styryl dye FM1-43 (Betz et al., 1992). Using this approach, we have analyzed the interaction of ACh released from a bouton onto receptors and compared it with Monte Carlo simulations (Bartol et al., 1991). This has made it possible to determine whether transmission is likely to be mediated by a synaptic vesicle releasing its entire contents onto a small patch of receptors beneath a bouton.

MATERIALS AND METHODS

Preparation of tissues

Rats (AAW) (~250 g) were anesthetized with ether and killed by cervical fracture. An incision was made in the lower abdomen, and both pelvic ganglia, together with connective tissue containing the fine hypogastric nerves, were dissected free. The sheath was carefully stripped from the surface of the ganglia by gently teasing the sheath. The preparation was continuously perfused at the rate of 3 ml/min with a modified Tyrode's solution of the following composition (mM): NaCl, 123.4; KCl, 4.7; $MgCl_2$, 1.0; NaH_2PO_4, 1.3; $NaHCO_3$, 16.3; $CaCl_2$, 1.0; glucose, 7.8. The

Received for publication 16 January 1996 and in final form 7 January 1997.

Address reprint requests to Dr. M. R. Bennett, Department of Physiology (F13), University of Sydney, NSW 2006, Australia. Tel.: 61-2-9351-2034; Fax: 61-2-9351-4740; E-mail: maxb@physiol.su.oz.au.

0006-3495/97/04/1595/12 $2.00

temperature of the bath was maintained between 33°C and 34°C. The reservoir supplying the bath was continuously gassed with 95% O_2/5% CO_2, and the pH was maintained at 7.3. The extracellular calcium concentration ($[Ca^{2+}]_o$) was changed by altering the amount of $CaCl_2$ dissolved in the Tyrode's solution supplying the bath.

Visualization of boutons

The preparation was placed in Tyrode's solution containing 0.5 mM $[Ca^{2+}]_o$ for about 20 min. It was then bathed for 30 s in 3,3-diethyloxardicarbocyanine iodide (0.1 mM; $DiOC_2(5)$; Yoshikami and Okun, 1984) and then washed with modified Tyrode's solution for 3 min. Terminals were chosen by viewing the $DiOC_2(5)$ fluorescent image via an image intensifier camera (Panasonic) attached to an Olympus (BH2) microscope equipped with a rhodamine filter set; the image was then displayed on a video monitor (National). Preparations were viewed using a 50× long working distance objective (Olympus, ULWD-MS Plan 50). The adverse effects of $DiOC_2(5)$ and fluorescence on quantal secretion have previously been studied (Bennett et al., 1986). The concentration of $DiOC_2(5)$ was kept to less than 1 μM and the period of excitation to less than 2 min to minimize any adverse effects of $DiOC_2(5)$ excitation. The area of excitation was restricted to the region being examined. The field of fluorescing boutons was hand-drawn on the TV monitor screen as soon as their fluorescent profiles had been identified; excitation was then terminated and transmitted light used to view the same area. Structures such as blood vessels and connective tissues were then drawn onto the monitor; the recording electrode was then moved onto the field of the drawing of the boutons. Any shift of the boutons with respect to the drawing could finally be checked by refluorescing the boutons at the termination of the experiment.

Extracellular recording from boutons

The hypogastric nerve was gently sucked into a pipette filled with modified Tyrode's solution. A silver/silver chloride wire on the inside of the pipette and one on the outside was used to stimulate the nerve, using square wave pulses of 0.08-ms duration and 10–20-V amplitude. The axons were stimulated continually at 0.2 Hz. Extracellular recordings of the terminal action potential and the EPSCs were obtained using microelectrodes (3–5-μm diameter, typically 4 μm) filled with the modified Tyrode's solution. These electrodes had a frequency bandwidth greater than 2 kHz. On some occasions, microelectrodes of 10-μm diameter were used on isolated boutons; these gave the same temporal characteristics for the EPSCs as those recorded with the smaller diameter electrodes. Focal extracellular recordings were obtained by placing the electrode over a visualized bouton. The EPSCs and the electrical signs of the terminal action potential could be observed on the oscilloscope while stimulating the hypogastric nerve. The position of the electrode rim with respect to the visualized boutons was adjusted to increase the amplitude of both the action potential and the EPSCs.

Data analysis

Between 100 and 200 stimuli were recorded on an Axoclamp-2A amplifier (Axon Instruments) and collected on a Macintosh microcomputer using a MacLab/4 interface and Scope software (version 3.3.3, AD Instruments, Sydney, Australia). The frequency bandwidth of the amplifier was 10 kHz. Translate 3.0 (AD Instruments, Sydney, Australia) was used to convert the Scope data files to Igor Pro 2.0 (WaveMetrics, Sydney, Australia) format for further analysis. Histograms of the EPSC amplitudes versus frequency were constructed.

The question arises as to whether the microelectrodes, of about 4μm diameter and filled with Tyrode's solution, allow recording of the EPSC without removing its high-frequency components. To test this, an electrical equivalent circuit of the microelectrode placed over a bouton, together with the underlying neuron soma on which transmitter acts, was constructed (Fig. 1 *A*). The current (EPSC) through the element R_s of the circuit was

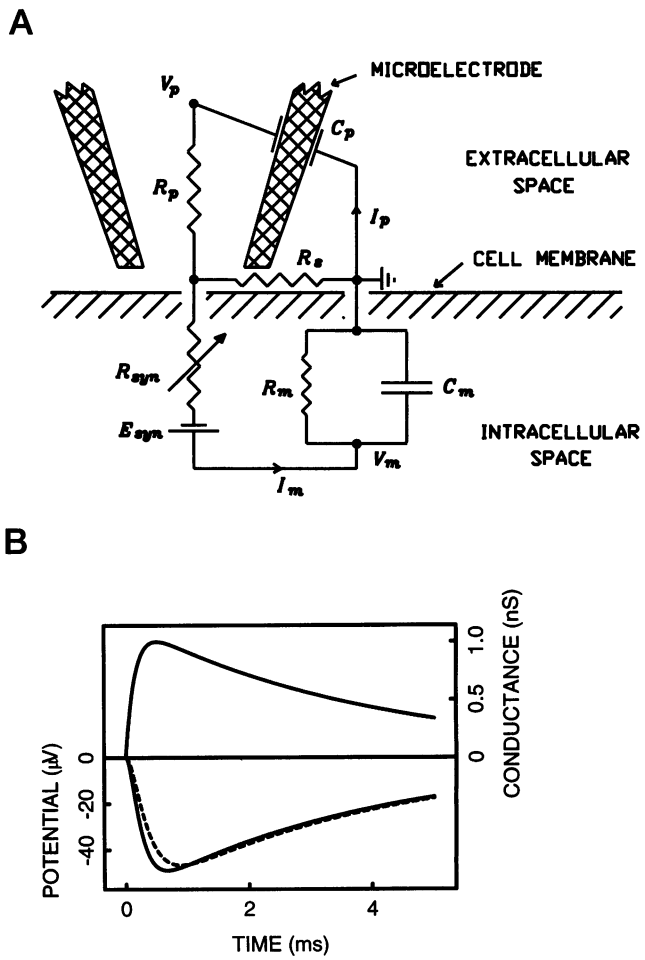

FIGURE 1 (*A*) Schematic diagram of the cell membrane, microelectrode tip, and equivalent electrical circuit. R_p and C_p are the resistance and capacitance of the pipette; R_s is the resistance of the extracellular fluid between the electrode tip and the membrane; R_m and C_m are the membrane resistance and capacitance. The synaptic input is represented by a variable resistance, $R_{syn}(t) = 1/G_{syn}(t)$, in series with a driving potential E_{syn}. I_p and I_m are the currents in the extracellular and the intracellular spaces respectively; V_m is the membrane potential and V_p is the potential inside the pipette, both measured relative to the potential of the extracellular fluid outside the pipette. (*B*) The microelectrode potential calculated using the circuit in *A*. The input is governed by the conductance $G_{syn}(t) = 1.176 \times G_{max}(\exp(-0.25t) - \exp(-6.88t))$, where $G_{max} = 1.0 \times 10^{-9}\ \Omega^{-1}$ and t is the time in milliseconds; the time course of $G_{syn}(t)$ is shown in the upper half of the figure. The remaining parameters have values $R_p = 5 \times 10^5\ \Omega$, $R_s = 1.0 \times 10^6\ \Omega$, $R_m = 5.0 \times 10^7\ \Omega$, $C_m = 1.0 \times 10^{-10}$ F, $E_{syn} = 0.05$ V. The lower half of the figure shows the time course of the potential V_p for $C_p = 75 \times 10^{-12}$ F (——) and for $C_p = 150 \times 10^{-12}$ F (– – –).

determined for a conductance change due to the action of a transmitter quantum ($1/R_{syn}$) that was represented by a double exponential with the same approximate time course as that measured, namely a time to peak of 0.5 ms and an exponential decay time constant of 4 ms (Fig. 1 *B*, *upper curve*). The approximate measured value of the electrode resistance R_p was 0.5 MΩ, and the frequency response of the electrode could be matched if it had a capacitance C_p of 75 pF. R_s was taken as about 1 MΩ, and the values of R_m and C_m from Kuba and Nishi (1979) and Griffith et al. (1980). The resulting EPSC peaked at about 0.65 ms (Fig. 1 *B*, *lower solid curve*); if C_p is doubled to 150 pF there is only a small further distortion of the calculated EPSC, which now peaks at 0.86 ms (Fig. 1 *B*, *broken curve*). Our measurements of the time to peak of the EPSC may be overestimated

by about 30%, because of the frequency response of the microelectrode, according to this analysis.

Monte Carlo simulation method

The kinetics of ACh interaction with receptors in the neurons of autonomic ganglia is governed by

$$2A + R \underset{k_{-1}}{\overset{2k_{+1}}{\rightleftharpoons}} A + AR \underset{2k_{-2}}{\overset{k_{+2}}{\rightleftharpoons}} A_2R \underset{\alpha}{\overset{\beta}{\rightleftharpoons}} A_2R^*, \quad (1)$$

where A is an ACh molecule, R is a receptor molecule containing a double site, AR is the singly bound molecule, A_2R is the doubly bound molecule, and A_2R^* is the bound molecule in the open conformation, corresponding to an open channel. As well as being used for the neuromuscular junction (Bartol et al., 1991), this scheme has been proposed for sympathetic neurons (Mathie et al., 1991) and parasympathetic neurons (Margiotta et al., 1987). The interaction of ACh with cholinesterase is taken to be (Bartol et al., 1991)

$$A + E \overset{k_3}{\longrightarrow} AE \overset{k_4}{\longrightarrow} E + Q, \quad (2)$$

where E denotes the esterase and Q the final products of hydrolysis.

To the above kinetic scheme must be added the spatial and temporal diffusion of the ACh molecules after quantal release. The Monte Carlo method involves following the motion of each molecule as it executes a random walk in free space, is reflected from presynaptic and postsynaptic membranes, and binds to or unbinds from receptor molecules. A detailed description and justification of the Monte Carlo method, as applied to the release of ACh in the neuromuscular junction, have been given by Bartol et al. (1991). The present calculations closely follow their methods.

The geometry of the system consists of two flat plates, taken to be 20 nm apart and shaped as squares with sides of 3.2 μm (compare figure 1 in Bennett et al., 1995a). Receptors are found only in a circular disc of diameter 0.41 μm located in the center of the postsynaptic membrane, giving a receptor area of 0.132 μm^2. The size chosen for the disc follows from the observation that the average length of the postsynaptic receptor cluster from random measurements of chord lengths through antibody-labeled clusters beneath a bouton on frog cardiac ganglia is 0.32 μm (Sargent and Pang, 1988, 1989; Sargent, 1993), so that the average diameter of such circular clusters is $(4/\pi)0.32 = 0.41$ μm.

Quantitative electron microscopic autoradiography indicates that there are about 5000 ^{125}I-neurotoxin F binding sites per μm^2 of membrane in dissociated cultured rat superior cervical ganglia (Loring et al., 1988), and about 600 ^{125}I-neurotoxin F binding sites per μm^2 in the avian ciliary ganglion (Loring and Zigmond, 1987). The large difference in these values seems to arise from the 10-fold smaller amount of synaptic membrane estimated to be associated with binding of the toxin on the cultured sympathetic neurons compared with that of the intact ciliary ganglion (Loring et al., 1988). There are possible problems with the calculations of the density of F-toxin binding sites in the autoradiography estimations (Loring et al., 1988). These are calculated on the basis of total binding of the toxin to the neuronal membrane in the vicinity of boutons and estimates of the extent of total postsynaptic receptor cluster area per neuron taken from the areas of electron-dense membrane beneath boutons (for details of the method of calculation, see Matthews-Bellinger and Salpeter, 1978). But as Loring and Zigmond (1987) comment, "Because of uncertainties in some of these values, the final densities should be regarded as estimates that could be off by a factor of 2 or 3." The density of the receptor patch in the Monte Carlo simulations has been taken as 1400 sites/μm^2, which is about 30% of the estimate of 5000 sites/μm^2 given by Loring et al. (1988) and is thus closer to the estimates for the intact ciliary ganglion of 600 sites/μm^2; the diameter of the patch has been taken to be 0.41 μm. This has been done to obtain values for the peak A_2R^* during the EPSC of about 150 that agree with the values obtained experimentally using the ratio of conductances between the peak of the EPSC and that of a single ACh channel (Rang, 1981; Derkach et al., 1983; see Discussion) and to a lesser extent with the nonstationary fluctuation analysis used in the present work.

The receptor area is subdivided into tiles of appropriate size, depending on the assumed receptor density, each tile containing one receptor; the actual size of the receptor is 10 nm^2, which is much smaller than the tile size. The esterase is located in a plane midway between the presynaptic and postsynaptic membranes and occupies a full square of side 3.2 μm. Quanta of ACh are secreted at time $t = 0$ from a point on the presynaptic membrane directly opposite the center of the receptor patch. Each molecule is moved randomly, using a time step of 0.75 μs. The algorithms and formulas used are as described by Bartol et a]. (1991).

The main parameters used in the simulations are shown in Table 1. The values for the ACh diffusion coefficient and esterase rate constants come from Bartol et al. (1991). The remaining values for the rate constants are are from Mathie et al. (1991), assuming no cooperativity in the binding of the ACh molecules. All of these rate parameters ($k_{\pm 1}$, $k_{\pm 2}$, α, β, k_3, k_4) have been multiplied by a factor of 3 to allow for the higher temperature used in the present experiments (34°C, as opposed to 23–24°C used by Mathie et al., 1991). The receptor density was determined by requiring approximately 150 open channels at the peak of the EPSC (see Results below), and the esterase density was fixed at one-half of the receptor density. Because many of the values listed in Table 1 are not well

TABLE 1 Values of parameters used in the Monte Carlo calculations

Quantity	Symbol	Value	Reference
Diffusion coefficient	D	6.5×10^{-6} cm^2 s^{-1}	Bartol et al. (1991)
Rate constant for binding to receptors	$k_{+1} = k_{+2}$	2.04×10^7 M^{-1} s^{-1} (6.9×10^7 M^{-1} s^{-1})	Mathie et al. (1991) (Skok)
Rate constant for unbinding from receptors	$k_{-1} = k_{-2}$	4170 s^{-1} (3705 s^{-1})	Mathie et al. (1991) (Skok)
Rate constant for forward conformational change	β	81000 s^{-1} (6293 s^{-1})	Mathie et al. (1991) (Skok)
Rate constant for backward conformational change	α	3522 s^{-1} (894 s^{-1})	Mathie et al. (1991) (Skok)
Rate constant for binding to esterase	k_3	1.56×10^8 M^{-1} s^{-1}	Bartol et al. (1991)
Rate constant for hydrolysis	k_4	10800 s^{-1}	Bartol et al. (1991)
Receptor density		1400 μm^{-2}	See text
Esterase density		700 μm^{-2}	See text

established experimentally, a systematic exploration was undertaken in which parameter values were allowed to vary over wide ranges; the results of these calculations are given in the Appendix. Also given in Table 1 are rate constants for a single-binding scheme, following the method of Skok (1987); this scheme is further discussed below (see Discussion).

The time course of ACh release from a vesicle

In the Monte Carlo scheme of Bartol et al. (1991), the release of the full number of ACh molecules in a quantum is instantaneous; recent experimental evidence indicates that this is likely to be the case for the neuromuscular junction (Stiles et al., 1996). However, if release is gradual (Khanin et al., 1994; van der Kloot, 1995), then detailed modeling of the release process (Khanin et al., 1994) suggests that the number of molecules C_r released by time t could follow an exponential time course, given by

$$C_r = C_0\left\{1 - \exp\left(\frac{-t}{VL/[\pi r_0^2 D]}\right)\right\}, \quad (3)$$

where C_0 is the initial number of ACh molecules in the vesicle, V is the vesicle volume, L is the length of the pore joining the vesicle to the presynaptic membrane, r_0 is the pore radius, and D is the diffusion coefficient for ACh through the pore. Using the parameter values of van der Kloot (1995), this is

$$C_r = C_0(1 - \exp(-t/0.210)), \quad (4)$$

where t is in milliseconds. Release, governed by Eq. 4, is easily incorporated into the Monte Carlo scheme.

Variance of the number of open channels

Assume that under the release of a quantum of transmitter each receptor molecule has the same probability p of becoming an open channel, and further assume that all openings are independent. Then, for N receptors, the mean M and variance σ^2 of the number of open channels are given by the binomial expressions $M = Np$, $\sigma^2 = Np(1 - p)$. Thus

$$\sigma^2 = M - \frac{1}{N}M^2. \quad (5)$$

If i is the single-channel current, I is the total mean current, and σ_I^2 is the variance of the total current, then $I = Mi$, $\sigma_I^2 = \sigma^2 i^2$, and so Eq. 5 becomes

$$\sigma_I^2 = Ii - \frac{1}{N}I^2, \quad (6)$$

which is a relation derived by Sigworth (1980). The corresponding relation for voltage, under the assumption of constant electrode impedance, is

$$\sigma_V^2 = Vv - \frac{1}{N}V^2, \quad (7)$$

where V is the mean amplitude of the EPSC, σ_V^2 is its variance, and v is the voltage change for a single channel. From Eq. 7, v is the slope of the σ_V^2-V curve for small V; the peak of this curve occurs when $v - 2V/N = 0$, allowing N to be estimated according to

$$N = 2V_{peak}/v, \quad (8)$$

where V_{peak} is the amplitude giving the peak variance.

RESULTS

The excitatory postsynaptic current at sympathetic boutons

Excitatory postsynaptic currents (EPSCs) were recorded with extracellular electrodes of 4–5-μm diameter placed in the loose patch mode over single visualized boutons on the surface of monopolar pelvic ganglion cells during stimulation of the hypogastric nerve at 0.5 Hz (Fig. 2). The extracellular current signs of an impulse in the bouton followed each stimulus artefact, indicating that there was no failure of conduction into the bouton (Fig. 2). The results for 10 EPSCs in each of 10 different boutons were analyzed. The EPSC recorded at any particular bouton did not fluctuate much from impulse to impulse (Fig. 2). Amplitude-frequency histograms of the EPSC were typically Gaussian with a small variance (Fig. 3 *A*), which might indicate that the quantum of transmitter released has saturated the receptor patches beneath the bouton. The range of mean EPSC size was from 29 ± 4 μV to 63 ± 8 μV (±SD) over the 10 boutons. The noise SD ranged from 2.0 μV to 5.0 μV. The frequency histograms of both the time for the EPSC to reach its peak value and the time constant of the falling phase of the EPSC were also distributed as Gaussians (Figs. 3 *B* and C). The EPSC for different boutons had a time to peak of about 0.7 ms (0.74 ± 0.10 ms) and decayed along a single exponential with a time constant of about 4.0 ms (3.8 ± 0.4 ms). The EPSC was blocked by 100 μM hexamethonium in all 18 ganglion for which this was tested.

The decay time of the EPSC recorded with an intracellular electrode in sympathetic ganglia is invariant with a change in amplitude of the EPSC (Kuba and Nishi, 1979). It was therefore of interest to determine the decay time of the

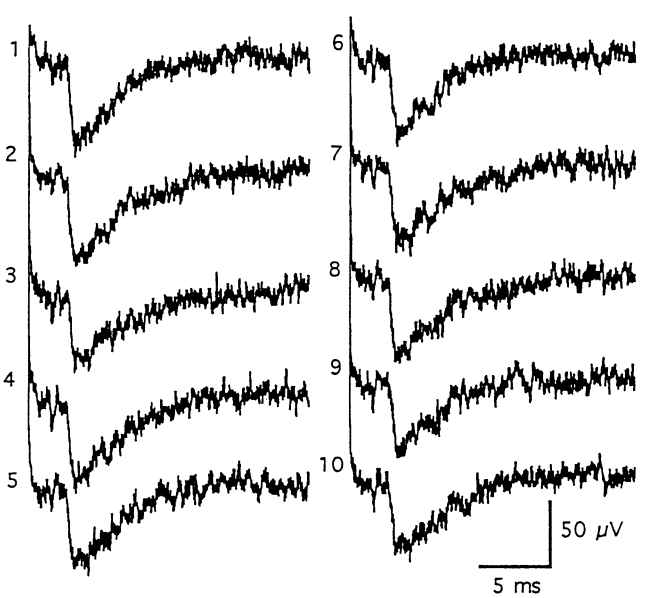

FIGURE 2 EPSCs recorded with a 4-μm extracellular electrode placed over a visualized bouton on the surface of a pelvic ganglion cell. Each of the records shows the EPSC preceded by an action potential in the bouton.

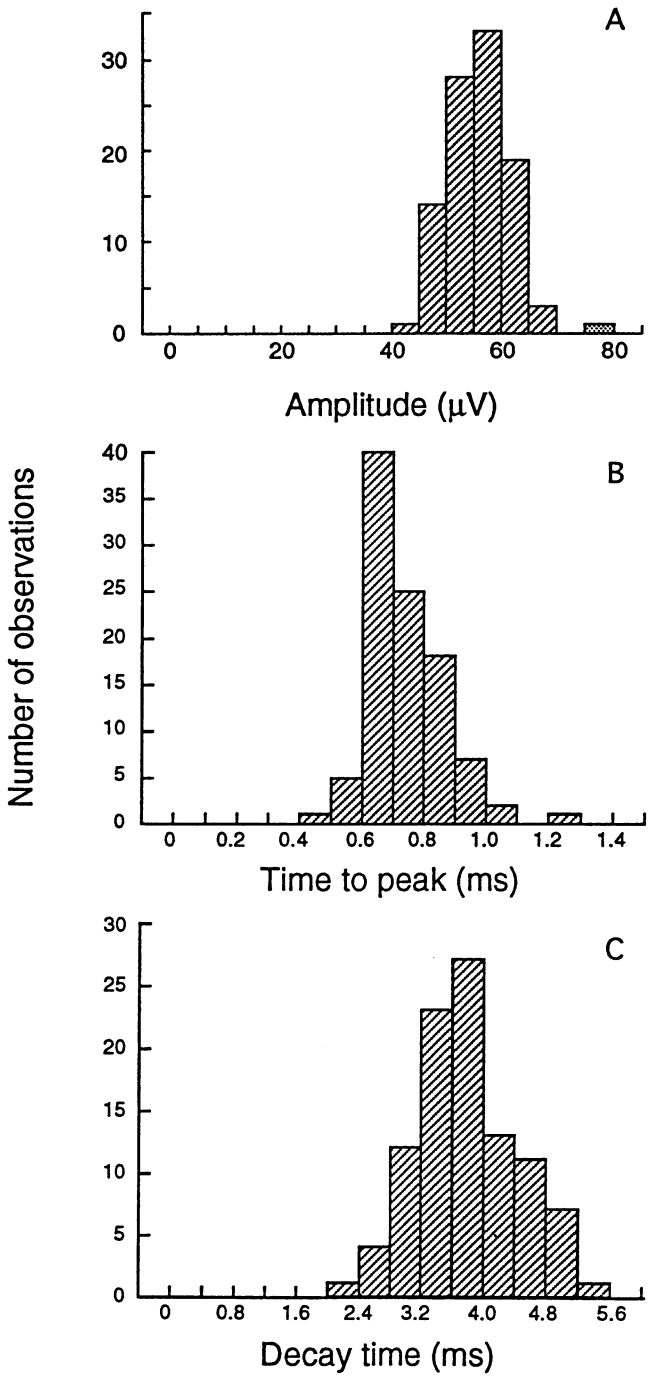

FIGURE 3 Characteristics of the EPSC. (*A*) Frequency histogram of EPSC amplitudes. (*B*) Frequency histogram of the times to peak. (*C*) Frequency histogram of the time constant of exponential decay of the EPSC. Results are for a single recording with a 4-μm electrode (n = 100 EPSCs).

EPSC recorded at a bouton as a function of the amplitude of the EPSC. Fig. 4 *B* shows that there was no consistent change in the decay time of the EPSC with the stochastic changes in amplitude recorded at a single bouton. The time to peak of the EPSC was also independent of the amplitude of the EPSC (Fig. 4 *A*).

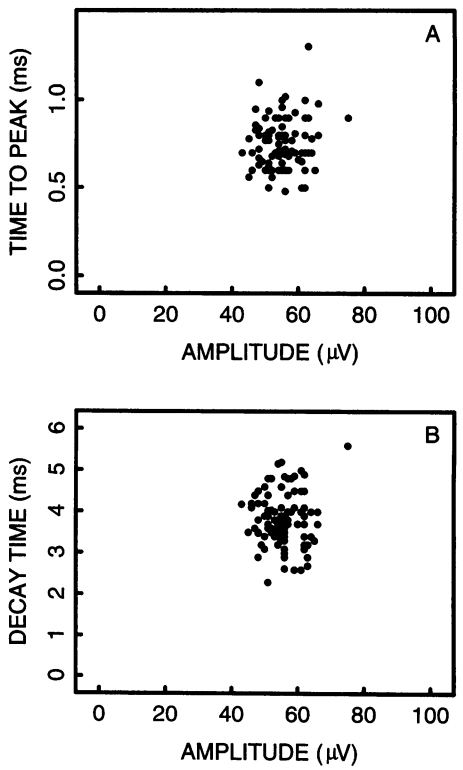

FIGURE 4 Relationship between the amplitude of EPSCs and their time to peak (*A*) or their time constant of decay (*B*). Results are for the same observations as shown in Fig. 3. Note that the time to peak and the time constant of decay are relatively constant for the range of amplitudes shown.

Reconstruction of the EPSC

The time course of the EPSC can be partially reconstructed if a quantum of ACh containing 9000 molecules is released from a bouton onto a receptor patch of 0.41 μm diameter which has a receptor density of 1400 μm^{-2}, and the ACh-receptor kinetics are those described in Materials and Methods (see the Appendix for the validation of these parameter values). Fig. 5 *A* shows that the number of ACh molecules declines rapidly over less than 0.1 ms, primarily because most of the ACh either escapes or is hydrolyzed by cholinesterase and to a smaller extent because of the binding of the ACh molecules to the receptors. Fig. 5 *B* shows the time course of the change in the number of open channels (A_2R^*) as well as of the doubly bound (A_2R) and singly bound receptors (AR) under these conditions. The number of open channels increases to a maximum value in about 0.2 ms and then declines exponentially with a time constant of about 4.0 ms. These temporal characteristics of the simulated EPSC are similar to those of the observed EPSC (compare Fig. 5 *B* with Fig. 2), except that the rise time is too short. The lack of dependence of the temporal characteristics of the experimental EPSC on its amplitude (Fig. 4) is also observed with the simulated EPSC. Thus the time to peak of the simulated EPSC shows only stochastic fluctuations around a mean of 0.2 ms with change in amplitude (Fig. 6 *A*, *points*), and the decay time fluctuates around a mean of 3.5 ms with change in amplitude (Fig. 6 *B*, *points*).

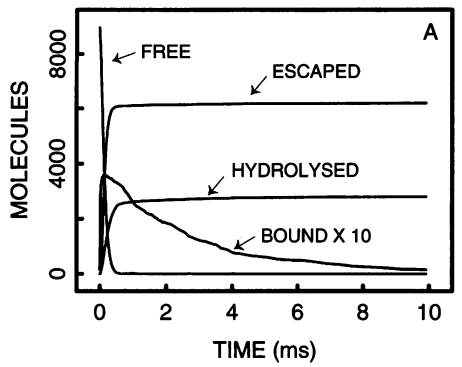

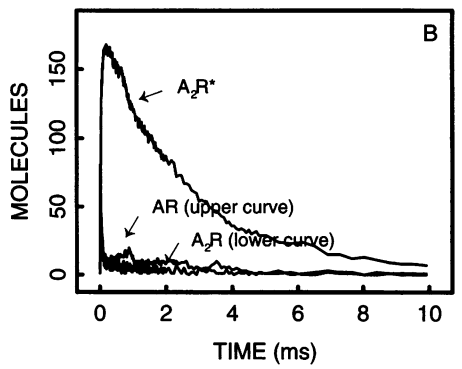

FIGURE 5 Theoretical time course of an EPSC at a bouton. ACh (9000 molecules) is released instantaneously at time $t = 0$ from a point 20 nm above the center of a circular receptor patch of 0.41 μm diameter containing a uniform distribution of receptors at a density of 1400 μm^{-2}. (*A*) The time course of bound ACh, as well as the number of free ACh molecules, the number hydrolyzed by cholinesterase, and the number that escape from the synaptic cleft. Note that BOUND has been multiplied by a factor of 10 to increase visibility. (*B*) The time course of singly bound receptors (*AR*), doubly bound receptors (A_2R), and open channels (A_2R^*). *AR* has a peak of 81 at about 11 μs, A_2R has a peak of 50 at about 15 μs, and A_2R^* has peak of 168 at about 200 μs.

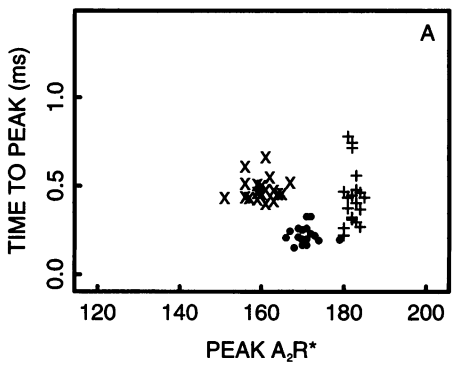

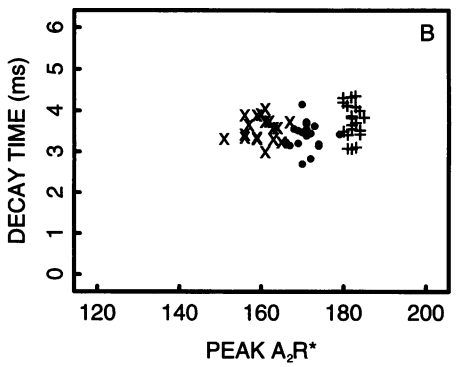

FIGURE 6 Theoretical changes in the time to peak (*A*) and the decay time (*B*) of the EPSC with changes in the amplitude of the EPSC. ●, Results from 20 separate Monte Carlo simulations with instantaneous release, as described in Fig. 5. ×, Corresponding results when the release is exponential with a time course of 0.210 ms, as given by Eq. 4. +, Corresponding results when the diffusion is slowed by an order of magnitude by taking $D = 6.5 \times 10^{-7}$ cm^2 s^{-1} and the forward rate constants are simultaneously reduced by a factor of 2 to $k_{+1} = k_{+2} = 1.02 \times 10^7$ M^{-1} s^{-1}.

The experimentally observed rise times of 0.5–1.0 ms are not accommodated by the two-step binding given by Eq. 1, using the parameter values of Mathie et al. (1991) as given in Table 1. The analysis of the frequency response of the microelectrode given in Materials and Methods shows that the experimental technique might increase the apparent time to peak by about 30%, but this is still not enough to bridge the gap between the observed time to peak and that determined by a two-step binding scheme. One way of increasing the rise time without drastically altering the other characteristics of the simulated EPSC is to utilize the slow release of ACh from a vesicle, as governed by Eq. 4. The time to peak now increases to about 0.5 ms (Fig. 6 *A*, *crosses*) with no change in the decay time (Fig. 6 *B*, *crosses*). However, because many parameter values are not well determined experimentally, a detailed investigation of the effect of varying them over ranges of values has been undertaken (see the Appendix). If the diffusion coefficient D is kept at its "standard" value of 6.5×10^{-6} cm^2 s^{-1}, then no reasonable combination of parameter values gives a sufficiently slow rise without destroying other agreements. But if the diffusion is slowed by an order of magnitude by taking $D = 6.5 \times 10^{-7}$ cm^2 s^{-1} and the forward rate constants are simultaneously reduced by a factor of 2 to $k_{+1} = k_{+2} = 1.02 \times 10^7$ M^{-1} s^{-1}, then the time to peak increases to a mean of about 0.43 ms (Fig. 6 *A*, *plusses*), the decay time remains unchanged (Fig. 6 *B*, *plusses*) and the peak number of open channels increases slightly to a mean of 182.

The Monte Carlo simulations also give the relationship between the peak amplitude of the EPSC (that is, the peak number of open channels, A_2R^*) and the amount of ACh released. Fig. 7 (*broken line*) shows that the peak A_2R^* increases with an increase in ACh release up to about 9000 molecules. At this release, the peak A_2R^* is about 178, which is 95% of the number of receptors beneath the bouton (the receptor patch being 0.41 μm in diameter and having a receptor density of 1400 μm^{-2}). For slow release governed by Eq. 4, the approach to saturation with an increase in the number of ACh molecules is less steep (Fig. 7, *solid line*), but for a quantal size of 9000 ACh molecules, about 85% of the channels beneath the bouton are open.

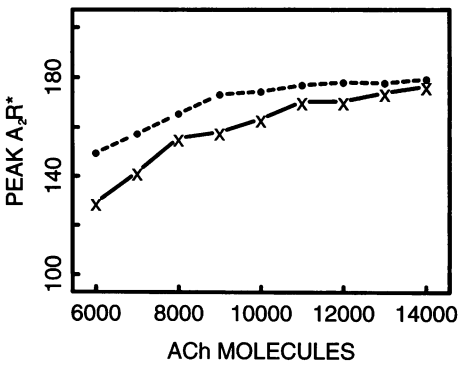

FIGURE 7 Theoretical increase in the maximum number of open channels (A_2R^*) during an EPSC with an increase in the amount of ACh released. The number of ACh molecules starts at 6000 and increases in steps of 1000 up to a maximum of 14,000; the remaining parameters are as for Fig. 5. ●, Results for instantaneous release; ×, results for exponential release (Eq. 4).

Stochastic properties of the EPSC

The variability in the EPSC due to the stochastic properties of transmitter-receptor interactions was next computed. Fig. 8 *A* shows the results of 10 different runs using the same parameters as in Fig. 5, except that slow, rather than instantaneous, release of ACh has been used. With the release of 9000 molecules of ACh there is not much variability in the amplitude of the response. The standard deviation (SD) for the responses is given in Fig. 8 *B*; this increases during the rising phase of the responses to reach a peak value and then rapidly undergoes a transient decline before once more increasing during the falling phase of the responses. Plotting the variance of the responses against their mean amplitude allows estimates to be made of the number of receptors beneath a bouton according to the nonstationary analysis of Sigworth (1980). This analysis depends on approximating the nonuniform application of a quantum of acetylcholine released by the bouton by a pulse of acetylcholine applied uniformly to the receptor patch beneath a bouton. Fig. 8 *C* shows such a plot using data from the falling phase of the simulated EPSC together with Sigworth's relation (Eq. 6, shown as a solid line), in which N, the number of receptors beneath a bouton as used in the simulations, is 185. There is reasonable agreement between the theoretical curve and the simulated stochastic variations in the number of A_2R^* up to the vicinity of the peak of the curve. This result for the falling phase encouraged us to use the Sigworth relation on the falling phase of experimental EPSCs. The average of 10 recorded EPSCs at a bouton together with their standard deviation are shown in Fig. 9, *A* and *B*; as in the Monte Carlo analysis, the standard deviation increases to a peak value during the rising phase of the EPSC, declines, and then increases again during the declining phase of the EPSC. Sigworth's relation (Eq. 6) between the variance and the average amplitude of the EPSC gives the curve shown in Fig. 9 *C*, which is drawn using the single-channel voltage $v = 0.32\ \mu V$ estimated from the initial slope of the experimental points and the receptor number $N = 120$ found from Eq. 8.

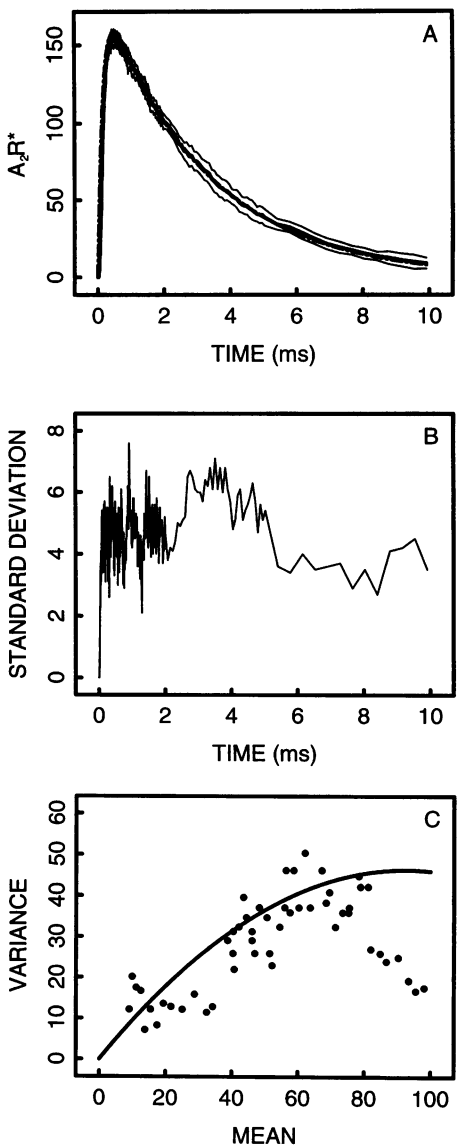

FIGURE 8 Stochastic variation in the Monte Carlo simulations of the response due to 9000 ACh molecules released over an exponential time course (Eq. 4) onto a 0.41-μm diameter patch containing receptors of density 1400 μm^{-2}. (*A*) The time course of A_2R^* for 10 different trials. The thick line gives the mean; the thin lines give upper and lower bounds of one standard deviation from the mean. (*B*) The SD of the 10 responses in *A*. (*C*) Relationship between the variance of the 10 responses in *A* and their mean value taken at different times on the falling phase; the continuous line is the Sigworth relation (see Materials and Methods) $\sigma^2 = M - M^2/N$, where M = mean A_2R^*, σ^2 = variance, and $N = 185$.

DISCUSSION

Parameter choice

Because many of the parameters values necessary for the Monte Carlo calculation of the EPSC are not well established, a number of runs were done using a range of values

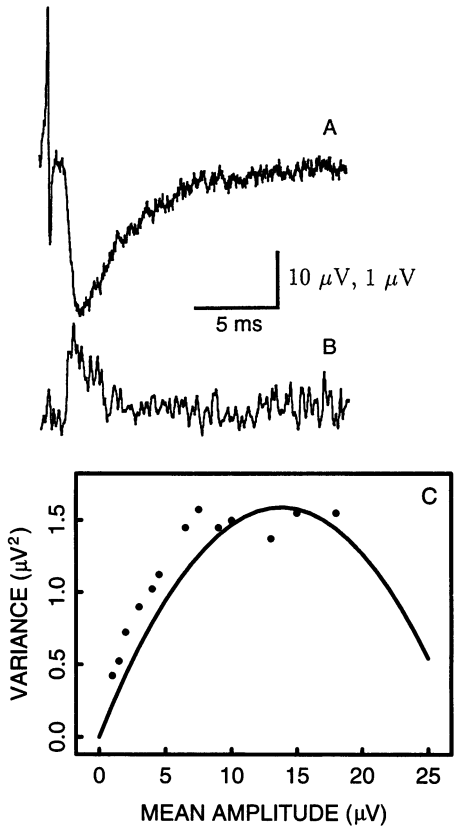

FIGURE 9 Experimentally observed variations in the size of the EPSC recorded with a 4-μm diameter electrode from a visualized bouton over 10 nerve impulses. (*A*) The time course of the mean of the 10 EPSCs; calibration is 10 μV. (*B*) The standard deviation of the responses in *A*; calibration is 1 μV. (*C*) A plot of the variance of the EPSCs against their mean amplitude at different times in the falling phase; the continuous line is $\sigma_V^2 = 0.32V - V^2/120$, according to the Sigworth relation (Eq. 5).

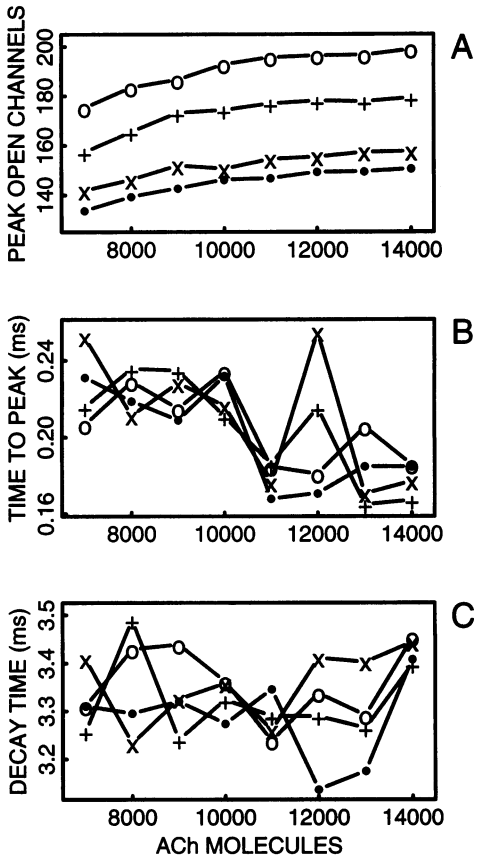

FIGURE 10 Characteristics of the simulated EPSC as a function of the number of ACh molecules released instantaneously at $t = 0$ for several receptor densities. The remaining parameter values are as in Table 1, except that the esterase density is always taken to be one-half of the receptor density. Receptor densities used are (μm^{-2}): 1200 (●), 1300 (×), 1400 (+), 1500 (○). Each point given on the graphs is the average of 10 Monte Carlo simulations. (*A*) Peak number of open channels. (*B*) Time to peak. (*C*) Decay time.

of ACh molecules released, receptor and esterase densities, and rate constants. The results of this exploration of the parameter space are given in the Appendix, together with a discussion of the choice of parameters used in the simulations.

It has been proposed by some that the kinetics of ACh interaction with receptors in the neurons of autonomic ganglia can be described in terms of a single binding followed by a configurational change (Derkach et al., 1987; Skok, 1987):

$$A + R \underset{k_{-1}}{\overset{k_{+1}}{\rightleftharpoons}} AR \underset{\alpha}{\overset{\beta}{\rightleftharpoons}} AR^*, \qquad (9)$$

where AR* now denotes an open channel. Monte Carlo simulations using this scheme indicated that, with some parameter adjustment from the values given by these authors (k_{+1} and k_{-1} were corrected for temperature by multiplying by 3; β and α were not changed—the values used are given in brackets in Table 1), it was possible to reproduce the main features of the experimental EPSCs: specifically, a peak of 155 open channels, a time to peak of 0.56 ms, and a decay time of 3.50 ms. It may seem surprising that a single-binding scheme leads to a longer rise time than a double-binding scheme, but in the present case the difference lies essentially in the rate of the configurational change: the values of β and α given by Mathie et al. (1991) are much larger than those given by Skok (1987). Reducing the Mathie values to well below their temperature-corrected values does finally give some increase in rise time, but this is accompanied by an unacceptable increase in decay time and a substantial fall in the peak number of open channels (see the Appendix and, in particular, Fig. 12).

In spite of the fact that the single-binding scheme can give agreement, this is not the favored mechanism; it seems most likely that the interaction of ACh with receptors in autonomic ganglia is like that at the neuromuscular junction—namely it is governed by a two-step binding scheme, as in Eq. 1 (Margiotta et al., 1987; Mathie et al., 1991).

Receptors

The question arises as to how many receptor clusters and indeed active zones may be associated with the boutons

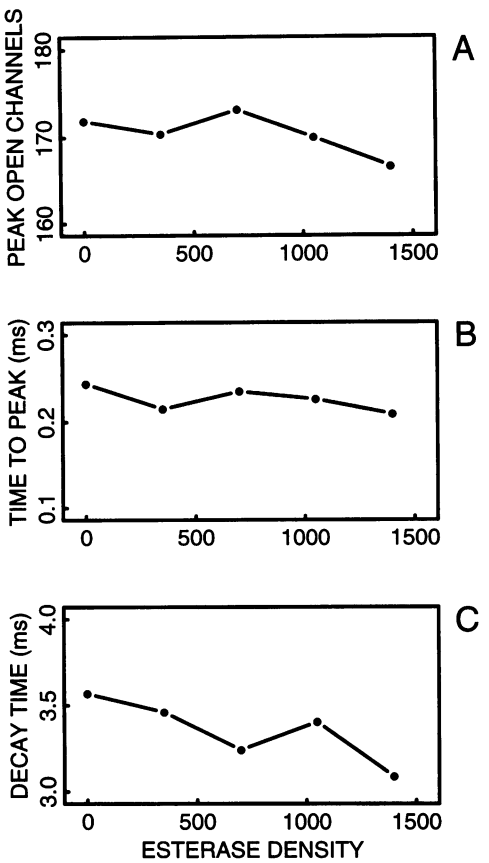

FIGURE 11 Characteristics of the simulated EPSC as a function of the esterase density. ACh (9000 molecules) is released instantaneously; the remaining parameter values are as in Table 1. Each point given on the graphs is the average of 10 Monte Carlo simulations. (*A*) Peak number of open channels. (*B*) Time to peak. (*C*) Decay time.

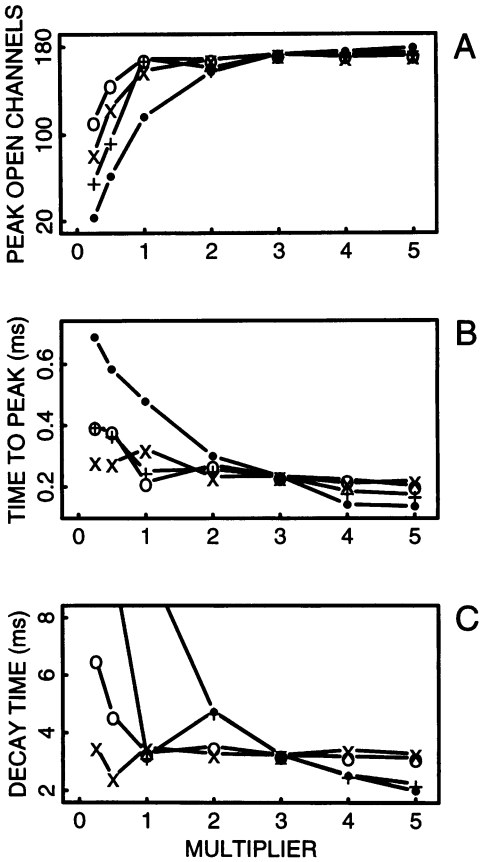

FIGURE 12 Dependence of the simulated EPSC on the values of the rate constants. The pairs of rate constants (k_{+1}, k_{-1}; k_{+2}, k_{-2}; α,β) were varied while keeping their ratios (k_{+1}/k_{-1}, k_{+2}/k_{-2}, α/β) constant. The base values (multiplier = 1) are those of Mathie et al. (1991) (that is, one-third of the values given in Table 1). The multiplier is the factor multiplied times each member of the pair being varied; the remaining rate constants take the values given in Table 1. The cases considered are k_{+1}, k_{-1} varied (×); k_{+2}, k_{-2} varied (+); α, β varied (○); all three ratios varied simultaneously (●). Each point given on the graphs is the average of 10 Monte Carlo simulations. (*A*) Peak number of open channels. (*B*) Time to peak. (*C*) Decay time.

recorded from in the pelvic ganglion. Confocal microscopy of dextran-rhodamine-labeled boutons on the surface of these ganglion cells has shown that they are typically about 1–2 μm in diameter (Warren et al., 1995b). It is this class of boutons that has been studied in the present work. Boutons of this size should have at the most one active zone, according to the relationship between the number of active zones and bouton size derived for frog autonomic ganglia (see figure 2 in Streichert and Sargent, 1989). Such boutons in the frog ganglia possess a single receptor cluster, although an adjacent receptor cluster may occur about 1–2 μm away in a minority of cases (about 20%; Sargent and Pang, 1989). If these observations hold for the pelvic ganglion, then it seems likely that the EPSCs recorded in the present work were generated by transmitter release from single active zones onto single receptor patches. This is supported by the observation that amplitude-frequency histograms of EPSCs at single bouton recordings were described by a single Gaussian distribution.

Application of nonstationary fluctuation analysis (Sigworth, 1980) to the synaptic currents measured at single boutons gave an estimate of the number of receptor channels available for transmission of ~120. Given that the probability of any channel being open at the peak of the response is $I/(iN)$, where I is the total current and i is the single-channel current, or about 0.6, then about 70 channels are open at the peak of the response, according to the analysis of the experimental data. Conductance measurements give between 75 and 150 receptor channels open at the peak of the SEPSC. This is derived on the basis that the mean size of SEPSCs is due to a conductance change of ~3000 pS (Rang, 1981; Derkach et al., 1983; Hirst and McLachlan, 1984) and that a single synaptic acetylcholine receptor has a conductance of 30 pS (Derkach et al., 1983; Rang, 1981). There is then general agreement between the estimates for the number of available receptor channels at a bouton based on electrophysiological analyses. There are, however, some caveats concerning these calculations. First, the conductance of the acetylcholine receptor-channel complex has only been determined thus far by noise analysis of the effects of exogenous acetylcholine (Rang, 1981), so it is likely that the conductance measurements are for extrasyn-

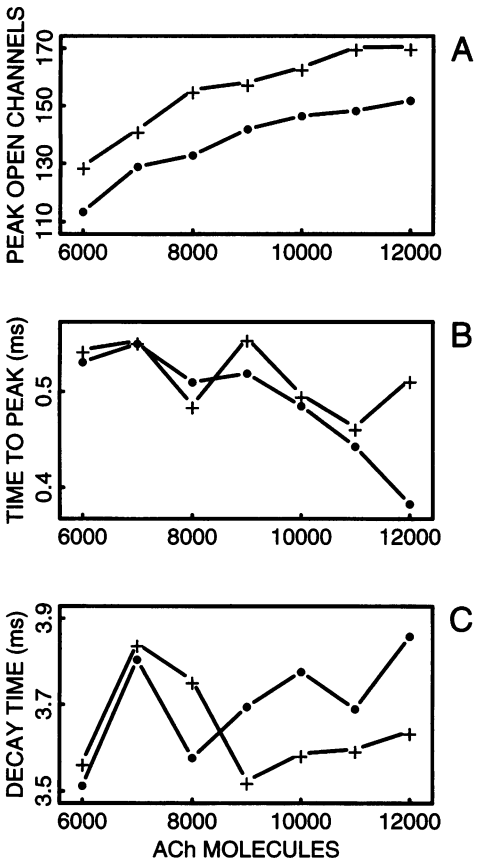

FIGURE 13 Characteristics of the simulated EPSC as a function of the number of ACh molecules released for exponential release according to Eq. 4. Results are shown for receptor densities of 1300 μm^{-2} (●) and 1400 μm^{-2} (+), the esterase density being set to one-half the receptor density in each case. The remaining parameter values are as in Table 1. Each point given on the graphs is the average of 10 Monte Carlo simulations. (*A*) Peak number of open channels. (*B*) Time to peak. (*C*) Decay time.

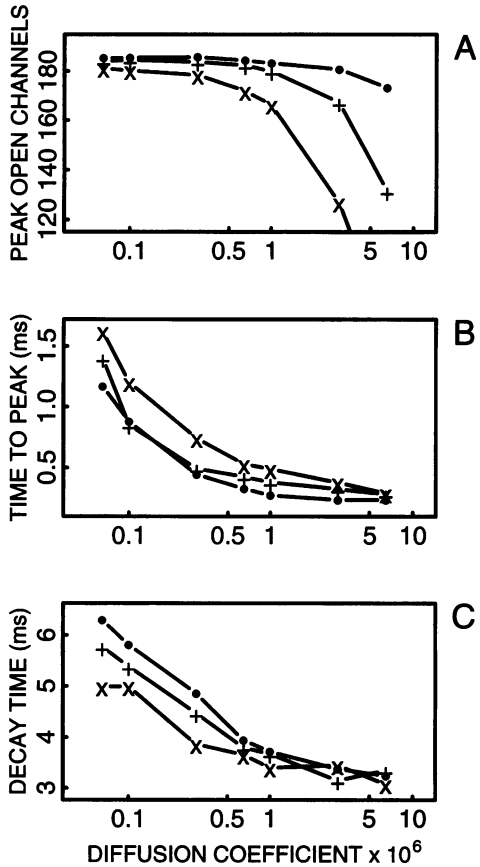

FIGURE 14 Characteristics of the simulated EPSC as a function of the diffusion coefficient *D*. Results are shown for the remaining parameters as in Table 1 (●), and for k_{+1}, k_{+2} reduced to one-half (+) and one-quarter (×) of their values in Table 1. Each point given on the graphs is the average of 10 Monte Carlo simulations. (*A*) Peak number of open channels. (*B*) Time to peak. (*C*) Decay time.

aptic acetylcholine receptors, which may be different from synaptic acetylcholine receptors. Second, the acetylcholine noise measurements on rat submandibular ganglion cells reveal two kinetic components at 20°C, one with a time constant of 5–9 ms and the other with a time constant of 27–45 ms (Rang, 1981). Although the evoked EPSC contains both time constants, the spontaneous EPSC only has the fast time constant, suggesting that it arises from activation of a different set of receptors than does the evoked EPSC. Acetylcholine noise measurements on rabbit sympathetic neurons at 35°C also reveal two kinetic components with time constants of 1.1 ms and 5.0 ms (Derkach et al., 1983). In this case, both spontaneous and evoked EPSCs possess only the slow time constant. It is possible in this case that the pool of about 100 receptor-channel complexes at synapses only consists of the slow channel and that the fast receptor channel is extrasynaptic.

Time course of EPSCs

There is general agreement between the time to peak and the decay time of the EPSC recorded at boutons and the SEPCs recorded with an intracellular electrode in autonomic ganglia. At 34°C the time to peak averaged 0.7 ms and the time constant of decay was 4 ms. The time constant of decay of the SEPSC for other autonomic ganglia is 4.5 ms for rabbit at 34°C (Derkach et al., 1983), 5–9 ms for rat at 20°C (Rang, 1981), and 4.5 ms in frog at 24°C (Kuba and Nishi, 1979; MacDermott et al., 1980)). Kuba and Nishi (1979) obtained a rise time of 1.87 ms for the EPSC in frog sympathetic ganglia and made the additional interesting observation that the decay time of the EPSC was unaffected by a change in the EPSC amplitude. This latter observation was confirmed for recordings from single boutons in the present work, in which the stochastic variations in the amplitude of the EPSC were unaccompanied by changes in the temporal characteristics of the EPSC.

The Monte Carlo simulations of the EPSC, using the kinetic constants for ACh-receptor interaction estimated at 23–24°C by Mathie et al. (1991) (and adjusted for temperature using a Q_{10} of 3), together with the receptor patch characteristics discussed above, gave a time to peak of the EPSC of about 0.25 ms and a time constant of decay of about 3.5 ms. Incorporating slow release of transmitter from

the vesicle increased the time to peak to about 0.5 ms without significantly altering the decay time, thus giving values similar to those observed experimentally. Furthermore, the Monte Carlo simulations showed no consistent variations in the rise time or the decay time of the EPSC with a change in amplitude, and this was also observed experimentally. In addition, the Monte Carlo simulations indicate that about 9000 ACh molecules give rise to the 150 or so open receptor channels at the peak of the EPSC. This number of ACh molecules is on the same order of magnitude as that estimated for the number of ACh molecules in a synaptic vesicle (Miledi et al., 1982; Whittaker, 1990). The model of transmission at a single sympathetic bouton that emerges from this study is that a very large excess of transmitter is released in a packet onto a relatively small receptor patch. Similar theoretical arguments that such a model is appropriate for central boutons have been made (Busch and Sakmann, 1990; Edwards, 1991), although recordings from single intact central boutons have yet to be achieved.

APPENDIX: EFFECTS OF PARAMETER CHANGES ON MONTE CARLO SIMULATION RESULTS

The parameter values used in most of the calculations are given in Table 1. With the incorporation of exponential release of transmitter according to Eq. 4, these give an EPSC that agrees with the experimental one. However, because a number of the parameter values are not well established experimentally, a systematic exploration of the effect of varying them was undertaken.

The effect of increasing the amount of ACh released for four different receptor densities is shown in Fig. 10. For all receptor densities, saturation is achieved by the release of about 10,000–12,000 molecules of ACh (Fig. 10 *A*); the time to peak shows some decrease with increasing ACh (Fig. 10 *B*), but the decay time shows no systematic variation (Fig. 10 *C*).

The effect of changing the esterase density is shown in Fig. 11. The conclusion is that the esterase is not playing a large role in the Monte Carlo simulations, as increasing its density over several orders of magnitude causes only a small drop in the peak number of open channels (Fig. 11 *A*) and a small decrease in decay time (Fig. 11 *C*); time to peak is almost unaffected (Fig. 11 *B*). A similar result has recently been obtained for the effects of changes in esterase density on the time course of endplate currents (Anglister et al., 1994). Fig. 12 shows the effects of varying the rate constants for the binding of the ACh to the receptors. Because six constants ($k_{\pm 1}$, $k_{\pm 2}$, α, β) are involved, varying them all independently was not feasible. Instead, because the ratios k_{+1}/k_{-1}, k_{+2}/k_{-2}, and α/β are better established experimentally than the individual values, these ratios were kept fixed at the experimentally determined values (Mathie et al., 1991), and pairs of values were varied, either individually or collectively. The parameters not being varied had the values given in Table 1; in Fig. 12 these correspond to a multiplier of 3, because the values in Table 1 have already been corrected for temperature by multiplication by 3. As can be seen from Fig. 12, *A–C*, small multipliers lead to considerable variation in the characteristics of the simulated EPSC, but for multipliers of 2 and above the variation is generally much less; then the main systematic trend is a decrease in the time to peak and in the decay time when k_{+2} and k_{-2} are increased (Fig. 12, *A* and *B*). Reducing the rate of the configurational change by reducing β and α had little effect when the multiplier was 1 or greater; below 1 there is some increase in the time to peak (Fig. 12 *B*), but this is accompanied by a sharp increase in the decay time (Fig. 12 *C*) and a substantial fall in the peak number of open channels (Fig. 12 *A*).

Fig. 13 shows the effects of varying the amount of ACh when release is exponential (Eq. 4) rather than instantaneous. The trends are similar to those found for instantaneous release (Fig. 10).

Finally, Fig. 14 shows the effects of slowing the diffusion by reducing the diffusion coefficient D below its "standard" value of 6.5×10^{-6} cm^2 s^{-1}. Reducing D alone by about an order of magnitude gives only a moderate increase in the time to peak (Fig. 14 *B*, *points*) but a substantial increase in the decay time (Fig. 14 *C*, *points*). However, if the forward rate constants k_{+1} and k_{+2} are also decreased, either to one-half (*plusses*) or one-quarter (*crosses*) of their standard values, then the increase in rise time is greater, whereas the increase in decay time is less.

Support under Australian Research Council grant AC9330365 is acknowledged.

REFERENCES

Anglister, L., J. R. Stiles, and M. M. Salpeter. 1994. Acetylcholinesterase density and turnover number at frog neuromuscular junctions, with modelling of their role in synaptic function. *Neuron.* 12:783–794.

Bartol, T. M., Jr., B. R. Land, E. E. Salpeter, and M. M. Salpeter. 1991. Monte Carlo simulation of miniature endplate current generation in the vertebrate neuromuscular junction. *Biophys. J.* 59:1290–1307.

Bennett, M. R. 1995. The origin of Gaussian distributions of synaptic potentials. *Prog. Neurobiol.* 46:331–350.

Bennett, M. R., L. Farnell, W. G. Gibson, and S. Karunanithi. 1995a. Quantal transmission at purinergic junctions: stochastic interaction between ATP and its receptors. *Biophys. J.* 68:925–935.

Bennett, M. R., W. G. Gibson, and J. Robinson. 1995b. Probabilistic secretion of quanta: spontaneous release at active zones of varicosities, boutons and endplates. *Biophys. J.* 69:42–53.

Bennett, M. R., P. Jones, and N. A. Lavidis. 1986. The probability of quantal secretion along visualized terminal branches at amphibian (*Bufo marinus*) neuromuscular synapses. *J. Physiol. (Lond.).* 379:257–274.

Betz, W. J., F. Mao, and G. S. Bewick. 1992. Activity-dependent fluorescent staining and destaining of living vertebrate motor nerve terminals. *J. Neurosci.* 12:363–375.

Bornstein, J. C. 1978. Spontaneous multiquantal release at synapses in guinea-pig hypogastric ganglia: evidence that release can occur in bursts. *J. Physiol. (Lond.).* 282:375–398.

Busch, C., and B. Sakmann. 1990. Synaptic transmission in hippocampal neurons: numerical reconstruction of quantal IPSCs. *Cold Spring Harb. Symp. Quant. Biol.* 55:69–80.

de Groat, W. C., and A. M. Booth. 1993. Synaptic transmission in pelvic ganglia. *In* Nervous Control of the Urogenital System. C. A. Maggi, editor. Harwood Academic Publishers, Sydney.

Derkach, V. A., R. A. North, A. A. Selyanko, and V. I. Skok. 1987. Single channels activated by acetylcholine in rat superior cervical ganglion. *J. Physiol. (Lond.).* 388:141–151.

Derkach, V. A., A. A. Selyanko, and V. I. Skok. 1983. Acetylcholine-induced current fluctuations and fast excitatory post-synaptic currents in rabbit sympathetic neurones. *J. Physiol. (Lond.).* 336:511–526.

Dryer, S. E., and V. A. Chiappinelli. 1987. Analysis of quantal content and quantal conductance in two populations of neurons in the avian ciliary ganglion. *Neuroscience.* 20:905–910.

Edwards, F. A. 1991. LTP is a long term problem. *Nature.* 350:271–272.

Griffith, W. H., J. P. Gallagher, and P. Shinnick-Gallagher. 1980. An intracellular investigation of cat vesical pelvic ganglia. *J. Neurophysiol.* 43:343–354.

Hirst, G. D., and E. M. McLachlan. 1984. Post-natal development of ganglia in the lower lumbar sympathetic chain of the rat. *J. Physiol. (Lond.).* 349:119–134.

Khanin, R., H. Parnas, and L. Segel. 1994. Diffusion cannot govern the discharge of neurotransmitter in fast synapses. *Biophys. J.* 67:966–972.

Kuba, K., and S. Nishi. 1979. Characteristics of fast excitatory postsynaptic current in bullfrog sympathetic ganglion cells. Effects of membrane potential, temperature and Ca ions. *Pflügers Arch. Eur. J. Physiol.* 378:205–212.

Lavidis, N. A., and M. R. Bennett. 1992. Probabilistic secretion of quanta from visualized sympathetic nerve varicosities in mouse vas deferens. *J. Physiol. (Lond.).* 454:9–26.

Loring, R. H., D. W. Sah, S. C. Landis, and R. E. Zigmond. 1988. The ultrastructural distribution of putative nicotinic receptors on cultured neurons from the rat superior cervical ganglion. *Neuroscience.* 24: 1071–1080.

Loring, R. H., and R. E. Zigmond. 1987. Ultrastructural distribution of ^{125}I-toxin F binding sites on chick ciliary neurons: synaptic localization of a toxin that blocks ganglionic nicotinic receptors. *J. Neurosci.* 7:2153–2162.

MacDermott, A. B., E. A. Connor, V. E. Dionne, and R. L. Parsons. 1980. Voltage clamp study of fast excitatory synaptic currents in bullfrog sympathetic ganglion cells. *J. Gen. Physiol.* 75:39–60.

Margiotta, J. F., D. K. Berg, and V. E. Dionne. 1987. The properties and regulation of functional acetylcholine receptors on chick ganglion neurons. *J. Neurosci.* 7:3612–3622.

Martin, A. R., and G. Pilar. 1964. Quantal components of the synaptic potential in the ciliary ganglion of the chick. *J. Physiol. (Lond.).* 175: 1–16.

Mathie, A., S. G. Cull-Candy, and D. Colquhoun. 1991. Conductance and kinetic properties of single nicotinic acetylcholine receptor channels in rat sympathetic neurones. *J. Physiol. (Lond.).* 439:717–750.

Matthews-Bellinger, J., and M. M. Salpeter. 1978. Distribution of acetylcholine receptors at frog neuromuscular junctions with a discussion of some physiological implications. *J. Physiol. (Lond.).* 279:197–213.

Miledi, R., P. C. Molenaar, R. L. Polak, J. W. Tas, and T. van der Laaken. 1982. Neural and non-neural acetylcholine in the rat diaphragm. *Proc. R. Soc. Lond. B.* 214:153–168.

Rang, H. P. 1981. The characteristics of synaptic currents and responses to acetylcholine of rat submandibular ganglion cells. *J. Physiol. (Lond.).* 311:23–55.

Sargent, P. B. 1993. The diversity of neural nicotinic acetylcholine receptors. *Annu. Rev. Neurosci.* 16:403–443.

Sargent, P. B., and D. Z. Pang. 1988. Denervation alters the size, number, and distribution of clusters of acetylcholine receptor-like molecules on frog cardiac ganglion neurons. *Neuron.* 1:877–886.

Sargent, P. B., and D. Z. Pang. 1989. Acetylcholine receptor-like molecules are found in both synaptic and extrasynaptic clusters on the surface of neurones in the frog cardiac ganglion. *J. Neurosci.* 9:1062–1072.

Sigworth, F. J. 1980. The variance of sodium current fluctuations at the node of Ranvier. *J. Physiol. (Lond.).* 307:97–129.

Skok, V. I. 1987. Nicotinic acetylcholine receptors in the neurones of autonomic ganglia. *J. Auton. Nerv. Syst.* 21:91–99.

Stiles, J. R., D. van Helden, T. M. Bartol, E. E. Salpeter, and M. M. Salpeter. 1996. Miniature endplate current rise times less than 100 microseconds from improved dual recordings can be modeled with passive acetylcholine diffusion from a synaptic vesicle. *Proc. Natl. Acad. Sci. USA.* 93:5747–5752.

Streichert, L. C., and P. B. Sargent. 1989. Bouton ultrastructure and synaptic growth in a frog autonomic ganglion. *J. Comp. Neurol.* 281: 159–168.

Tabatabai, N., A. M. Booth, and W. C. de Groat. 1986. Morphological and electrophysiological properties of pelvic ganglion cells in the rat. *Brain Res.* 382:61–70.

van der Kloot, W. 1995. The rise times of miniature endplate currents suggest that acetylcholine may be released over a period of time. *Biophys. J.* 69:148–154.

Warren, D., N. A. Lavidis, and M. R. Bennett. 1995a. Quantal secretion recorded from visualized boutons. *Neurosci. Lett.* 192:205–208.

Warren, D., N. A. Lavidis, and M. R. Bennett. 1995b. Quantal secretion recorded from visualized boutons on rat pelvic ganglion neurones. *J. Auton. Nerv. Syst.* 56:175–183.

Whittaker, V. P. 1990. Cholinergic synaptic vesicles are metabolically and biophysically heterogeneous even in resting terminals. *Brain Res.* 511: 113–121.

Yakota, R., and G. Burnstock. 1983. Synaptic organization of the pelvic ganglion in the guinea-pig. *Cell Tissue Res.* 232:379–397.

Yoshikami, D., and L. M. Okun. 1984. Staining of living presynaptic nerve terminals with selective fluorescent dyes. *Nature.* 310:53–56.